Carbon 98 (2016) 468–473

Contents lists available at ScienceDirect

Carbon

journal homepage: www.elsevier.com/locate/carbon

Novel three dimensional topological nodal line semimetallic carbon

Yong Cheng [a], Jinglian Du [a], Roderick Melnik [b], Yoshiyuki Kawazoe [c, d], Bin Wen [a, *]

[a] State Key Laboratory of Metastable Materials Science and Technology, Yanshan University, Qinhuangdao 066004, China
[b] The MS2Discovery Interdisciplinary Research Institute, Wilfrid Laurier University, 75 University Ave. West, Waterloo, Ontario N2L 3C5, Canada
[c] New Industry Creation Hatchery Center, Tohoku University, 6-6-4 Aramaki-aza-Aoba, Aoba-ku, Sendai 980-8579, Japan
[d] Institute of Thermophysics, Siberian Branch of the Russian Academy of Sciences, 1, Lavyrentyev Avenue, Novosibirsk 630090, Russia

ARTICLE INFO

Article history:
Received 23 July 2015
Received in revised form
9 October 2015
Accepted 11 November 2015
Available online 1 December 2015

ABSTRACT

A new cubic three dimensional carbon phase has been predicted by first-principles calculations. This phase is constructed by triangle graphene sheets, and dubbed as sc-C_{96}. The investigation on its electronic properties has indicated that sc-C_{96} possesses a topological nodal line semimetal state, which protected by the combination of time reversal and spatial inversion symmetries, and negligible spin–orbit interaction. Due to the cubic symmetry, the Fermi surface of sc-C_{96} is constituted of three nodal line circles. From the cohesive energy and phonon spectra, we find that sc-C_{96} is dynamically stable and may be easily synthesized by polymerizing C_{96} fullerene molecules at a relatively low pressure conditions (~1 GPa).

© 2015 Elsevier Ltd. All rights reserved.

1. Introduction

Topological semimetals, newly proposed nontrivial quantum materials [1–8], have attracted increasing attention due to their interesting quantum phenomena, physical properties (e.g. Fermi arcs on the side surfaces [9], unusually high bulk carrier mobility [10], and oscillating quantum spin Hall effect [11]) as well as great potential applications in future functional devices. As a typical example of topological semimetal carbon, graphene [12] possesses more superior comprehensive properties than other topological semimetals, such as high thermal conductivity [13], high strength [14] and chemistry stability [15], among others. Since graphene is a two dimensional (2D) topological semimetal, it is natural to ask, what is its three dimensional (3D) analogue? Recently, much effort have been devoted to explore novel carbon allotropes [16–19], and theoretical studies of 3D topological semimetal indicated that carbon also can form into 3D topological semimetal structures [6,18,20], while there is no any 3D topological semimetal carbon has been synthesized to date. Therefore, further exploring new 3D topological semimetal carbons and finding their easily synthesis paths are urgently needed.

In this paper, a simple cubic 3D carbon allotrope called sc-C_{96} has been predicted by means of the first-principles calculations. Our calculated results indicated that sc-C_{96} is a 3D topological nodal line semimetal, whose Fermi surface is protected by the time reversal and spatial inversion symmetry, and weak spin–orbit coupling (SOC) strength. In addition, sc-C_{96} is a dynamically stable phase, and the low phase transformation energy barriers from C_{96} fullerene molecules to sc-C_{96} indicated that sc-C_{96} may be easily synthesized under relatively mild conditions.

2. Computational methods

The first-principles calculations are performed on the basis of density functional theory (DFT) [21,22], as implemented in the Vienna ab initio simulation package (VASP) [23,24]. The all-electron projector augmented wave (PAW) method [25] is adopted with $2s^2 2p^2$ treated as the valence electrons. The exchange-correlation potential is described by the local density approximation (LDA) [26]. A plane-wave cutoff energy of 500 eV has been used in this work. The k-point separation in Brillouin zone of the reciprocal space is sampled as $11 \times 11 \times 11$. The conjugate-gradient algorithm is used to relax the ions in their instantaneous ground-state, and the convergence threshold is set to be within 1×10^{-6} eV/atom. The phonon dispersion curve is computed through the direct supercell method [27], and the supercell is $2 \times 2 \times 1$. It is obtained through the VASP and PHONOPY code [28]. The first-principles molecular dynamics simulations are performed in the canonical (NVT) ensemble with a $2 \times 2 \times 1$ supercell, each simulation lasted for 6 ps, with a time step of 1 fs. The climbing image nudged elastic band

* Corresponding author.
E-mail address: wenbin@ysu.edu.cn (B. Wen).

http://dx.doi.org/10.1016/j.carbon.2015.11.039
0008-6223/© 2015 Elsevier Ltd. All rights reserved.

Table 1
The space group, optimized lattice parameters (a and c), mass density (ρ), cohesive energy (E_{coh}), and bulk modulus (B) for sc-C_{96}, graphite, and diamond at zero pressure, compared to the available experimental and other theoretical values.

Structure	Space groups	References	a (Å)	c (Å)	ρ (g/cm^3)	E_{coh} (eV/atom)	B (GPa)
Graphite	$P6/mmm$	Our work	2.446	6.624	2.325	8.998	284
		[30]	2.443	6.679	2.301	9.001	288
		Expt. [30].	2.460	6.642–6.716	2.770–2.280		286–319
Diamond	$Fd\bar{3}m$	Our work	3.534		3.617	9.006	461
		LDA [30]	3.530		3.625	9.004	460
		Expt. [31].	3.567		3.520		443
sc-C_{96}	$Pm\bar{3}m$	LDA	11.597		1.227	8.529	149

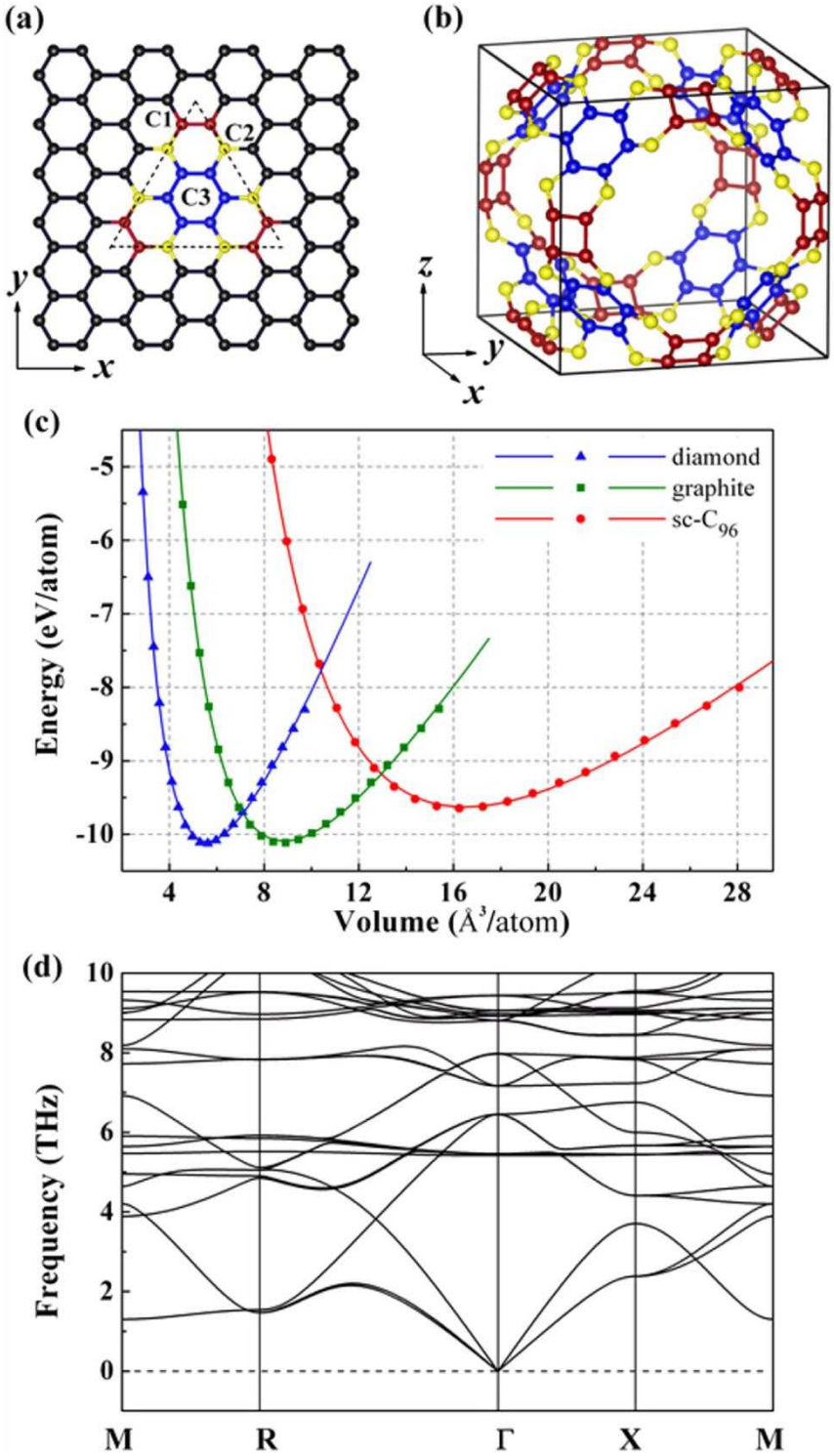

Fig. 1. (a) The basic building block of sc-C_{96} is a triangle graphene sheet (dashed area), the atoms located at the endpoints, sides and interior of the triangle graphene sheet are denoted as the C1, C2, C3 atoms and colored red, yellow, blue, respectively. (b) The optimized unit cell of sc-C_{96} that is interconnected by eight triangle graphene sheets. (c) Volume dependence of total energy for graphite, diamond, and sc-C_{96}. (d) Low-frequency part of phonon spectra for sc-C_{96}. The high symmetry q point path in the Brillouin zone is chosen as: M (1/2, 1/2, 0) → R (1/2, 1/2, 1/2) → Γ (0, 0, 0) → X (1/2, 0, 0) → M (1/2, 1/2, 0). (A color version of this figure can be viewed online.)

(CINEB) method [29] is used to simulate the phase transitions path. To verify the computational accuracy, benchmark calculations have been performed for diamond. The calculated lattice parameters and elastic constants (see Table 1) agreed well with the experimental and other theoretical values [30,31], confirming the reliability of our computational scheme.

3. Results and discussion

3.1. Structure and stability

Taking a triangle graphene sheet as the basic building block [Fig. 1(a)], a new carbon allotrope is built by combining eight blocks in a solid way, as displayed in Fig. 1(b). This allotrope possesses a simple cubic lattice and each unit cell contains 96 carbon atoms, which is thus coined as sc-C_{96}. By means of the first-principles calculations, the crystallographic parameters of sc-C_{96} have been optimized, and the results are listed in Table 1. It is found that the optimized lattice constant of sc-C_{96} is $a = 11.597$ Å, and the space group of sc-C_{96} is identified as $Pm\bar{3}m$ by checking the symmetry. Under this symmetry, there are three types of non-equivalent carbon atoms (denoted as C1, C2 and C3) in the structure of sc-C_{96}. The C1, C2 and C3 atoms are located at the endpoints, sides and interior of the triangle graphene sheet (see Fig. 1(a)), respectively, and their corresponding Wyckoff positions are (0.43140, 0.09378, 0), (0.33814, 0.17412, 0) and (0.28112, 0.19520, 0.10586). The bond lengths between C1 and C1 atoms are very close to that of diamond, and the remaining bond lengths are approximated by those of graphite. The detailed information of bond lengths and angles are given in Supplemental Table S1. Furthermore, because of very big cavity in the structure of sc-C_{96}, the density and bulk moduli of sc-C_{96} are only about 1.227 g/cm^3 and 149 GPa, respectively, which are much lower than in the case of diamond and graphite.

To investigate the thermodynamic stability of sc-C_{96}, the curve of volume dependence of total energy for sc-C_{96} has been fitted by Murnaghan's equation of state [32], and the results are plotted in Fig. 1(c). It can be seen that there is a single minimum in the corresponding curve of sc-C_{96}, signifying that sc-C_{96} is thermodynamically stable. By comparing the total energy of graphite, diamond and sc-C_{96}, it is noted that sc-C_{96} is less thermodynamically stable than graphite and diamond. The phonon spectra of sc-C_{96} have been also calculated to check the dynamic stability of sc-C_{96}, and the low-frequency part of phonon spectra for sc-C_{96} are presented in Fig. 1(d). It is found that there are no imaginary phonon modes, demonstrating that sc-C_{96} is a dynamically stable and energetically metastable structure. The highest phonon frequency of sc-C_{96} is about 46.77 THz (1559 cm^{-1}), which is higher than that of diamond (1324 cm^{-1}) and lower than that of graphite (1604 cm^{-1}) [33]. We have also found that there exist two narrow band gaps (46 and 73 cm^{-1}) in phonon spectra of sc-C_{96}, which could be useful in characterizing sc-C_{96}. Furthermore, first-principle molecular dynamics simulations at 300 K are also performed with a supercell of sc-C_{96} ($2 \times 2 \times 1$). It is noted that the structure of sc-C_{96} is kept after 6000 steps with a time step of 1 fs, which strongly demonstrates that sc-C_{96} is thermally stable at room temperature.

3.2. Electronic property

Now, let us turn to the electronic properties of sc-C_{96}. The calculated density of states (DOS) and band structure of sc-C_{96} are depicted in Fig. 2(a) and (b), respectively. From the band structure of sc-C_{96}, it can be observed that four electronic bands (I, II, III, IV) cross Fermi level, and the band I is degenerate at R_1 point, bands II, III and IV are triply-degenerate at R_2 point, resulting in a very small negative band gap (~64 meV) at R point near the Fermi level. It is also noted that the DOS near the Fermi level is 1.5 states/eV per cell, which is close to zero. Hence, sc-C_{96} is a kind of semimetallic carbon. Interestingly, there exists three pairs cross points [A and B, C and D, E and F (D and F are the same point due to the band degeneracy)] near the Fermi level along the X-R and R-M lines in the band structure of sc-C_{96} [see Fig. 2(c)], which is different from the graphene, whose conduction and valence band touch only at single point (Dirac point). In addition, we note that A and B have energy

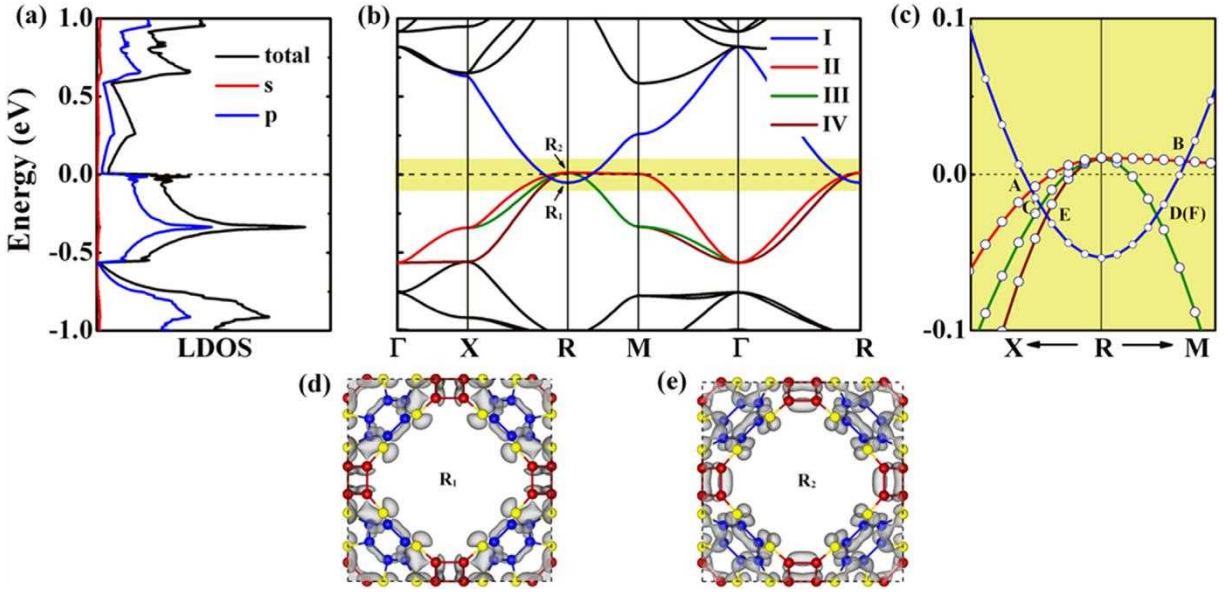

Fig. 2. (a) Density of states (DOS) of sc-C_{96} (b) Electronic band structures of sc-C_{96} without SOC. The letters R_1 and R_2 refer to the states of the highest valence band and the lowest conduction band at R high symmetry point, respectively. (c) The zooming band structures of sc-C_{96} in the energy dispersion near the Fermi level. The circles represent the weights of the C-p character. (d) and (e) show the band decomposed charge densities at R_1 and R_2 points, respectively. (A color version of this figure can be viewed online.)

dispersions around 20 meV, C and D have energy dispersions around 10 meV, E and F are at the same energy. To understand the origin of these cross points, the local density of states (LDOS) for sc-C_{96} has been calculated, and the result is presented in Fig. 2(a). As can be seen from LDOS of sc-C_{96}, the 2p orbital is predominant near Fermi level while the 2s orbital is quite small, suggesting that band I is π band, and bands II, III, and IV are π* bands. It was known that π and π* bands near the Fermi surface will induce the linear dispersion relation near the Fermi surface [34]. So the band crossings in sc-C_{96} is caused by π and π* bands, which is similar to that of graphene [35]. To further visualize the π and π* bands in the real space, the band decomposed charge density at R_1 and R_2 points have been calculated, and the results are plotted in Fig. 2(d) and (e), respectively. It can be clearly seen that the band decomposed charge density at R_1 and R_2 points show π bond features, which is consistent with our results from the LDOS.

3.3. Topological property

In order to explore the topological property of band structure of sc-C_{96}, the topological invariant, i.e. the Fermi surface of sc-C_{96}, has been calculated, and plotted in Fig. 3(a). The results show that the Fermi surface has eight parts around the corner of the Brillouin zone of sc-C_{96}, each part [see Fig. 3(b)] is formed by the electron pockets and hole pockets near Fermi level. Owning to the cubic symmetry of sc-C_{96}, the eight parts can be assembled into circular-like nodal lines, where R point is its center and parallel the $k_x = \pi/a$, $k_y = \pi/a$, $k_z = \pi/a$ plane [see Fig. 3(c)], respectively. This feature is similar to the band crossings behavior in Mackay-Terrones crystals and Cu_3PdN [6,7,18,36]. To further uncover the origin of these node-lines, the band crossings of band I and II, I and III, I and IV near the Fermi level in the $k_z = \pi/a$ plane have been calculated, as shown in Fig. 3(d), (e) and (f), respectively. It can be observed that the cross

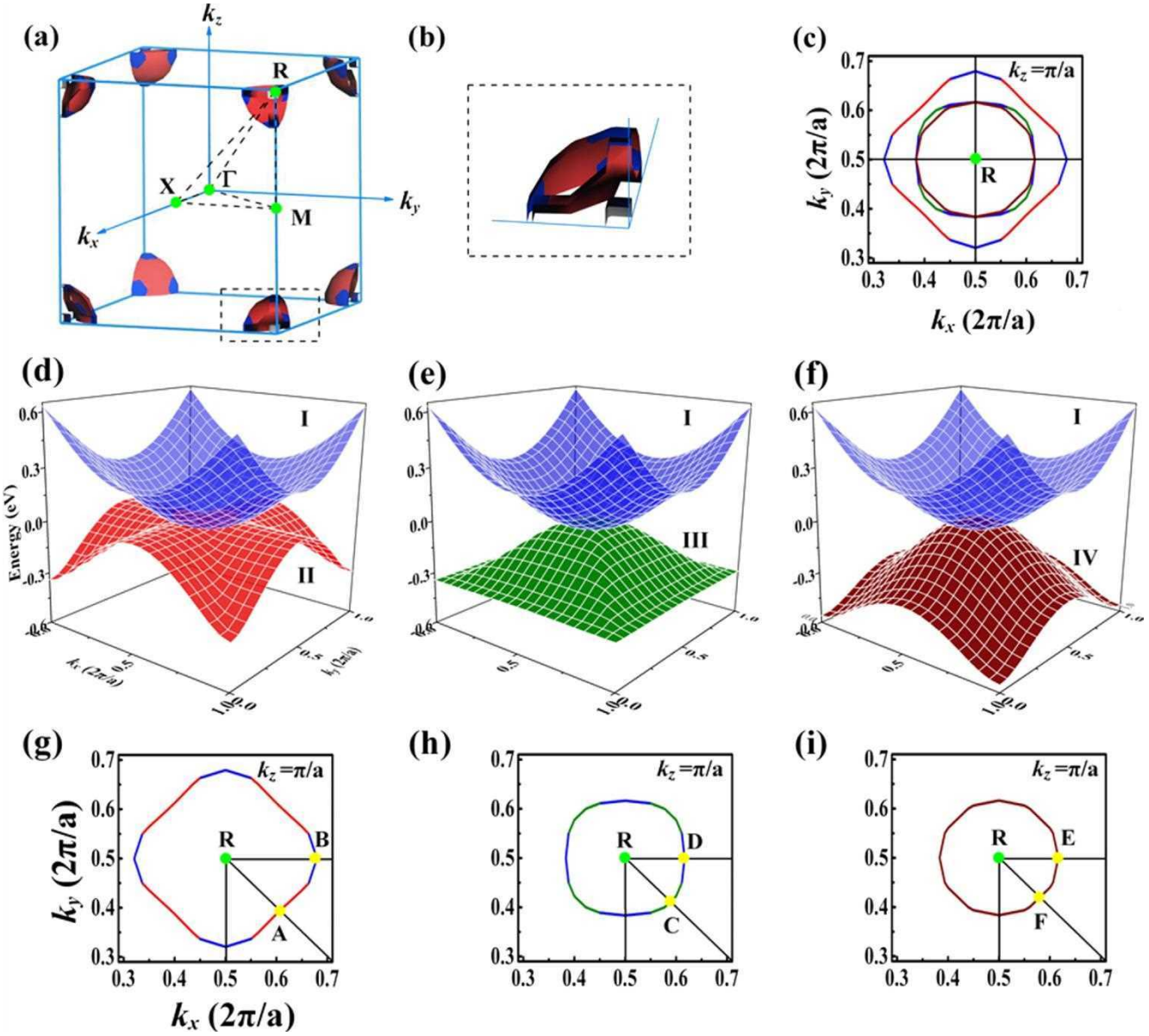

Fig. 3. (a) Fermi surface of sc-C_{96}, which consists of eight parts around the corner of the Brillouin zone. (b) The zooming part in Fermi surface of sc-C_{96}, which is formed by the node-like hole (blue) pockets and line-like electron (red) pockets near Fermi level. (d)–(f) show the band crossings behavior of band I and II, I and III, I and IV near the Fermi level in $k_z = \pi/a$ plane, respectively. (g)–(i) show the projective band crossings behavior corresponding to (d)–(f), the crossing happens at different eigen energy as indicated by different color, the blue lines indicate the lower energy region. (A color version of this figure can be viewed online.)

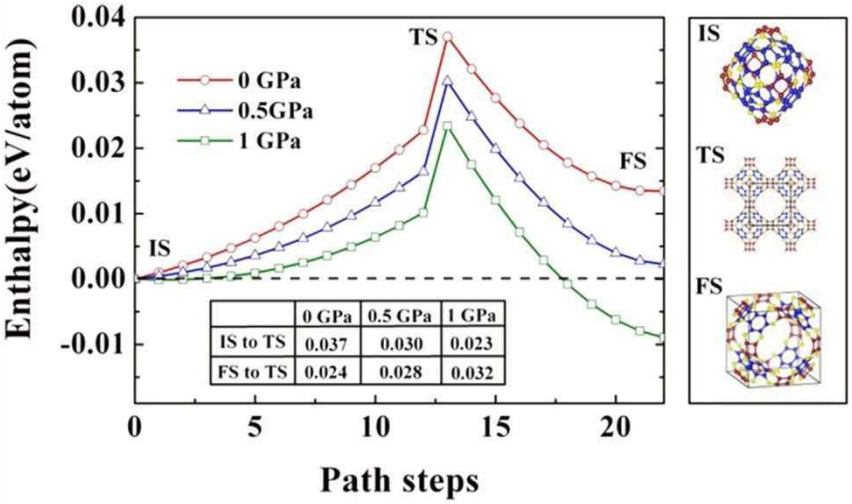

Fig. 4. Enthalpy vs pathway step for the transition from C_{96} fullerene molecules to sc-C_{96} at pressures of 0, 0.5, 1 GPa. The letter IS refers to the initial structure: C_{96} fullerene molecule containing 6 four-member rings (4-MRs) and 44 six-member rings (6-MRs), TS stands for the transition structure: C_{96} fullerene molecules are interconnected by 4-MRs, and FS is the final structure, i. e. sc-C_{96}. Energy barriers (in eV/atom) have been listed in the inset table. (A color version of this figure can be viewed online.)

points are located at a closed loops [see Fig. 3(g), (h) and (i)], forming the node-lines in $k_z = \pi/a$ plane, as shown in Fig. 3(c). Due to the mirror symmetry in sc-C_{96}, the situation in $k_x = \pi/a$ or $k_y = \pi/a$ plane are the same with $k_z = \pi/a$ plane, thus the band crossings in sc-C_{96} lead to the node-lines-like Fermi surface. Remarkably, when SOC is considered, we find that there is no dramatic change in the band structure of sc-C_{96}, as shown in Supplemental Fig. S1, and the SOC strength is about 0.2 meV, which can be neglected. Because the band structure of sc-C_{96} possesses both time reversal and spatial inversion symmetry, which meets another factor for topological semimetal, suggesting that sc-C_{96} is a new 3D topological nodal line semimetallic carbon.

3.4. Synthesis possibility

Finally, we propose a possible synthesis pathway to obtain such intriguing 3D topological nodal line semimetallic carbon by polymerizing C_{96} fullerene molecules. Fig. 4 shows the enthalpy vs pathway step for the transition from C_{96} molecules to sc-C_{96} under 0, 0.5 and 1 GPa. At the pressures of 0 and 0.5 GPa, the C_{96} molecule is energetically more favorable than sc-C_{96}, implying that the polymerization reaction does not satisfy thermodynamic conditions. At the pressure of 1 GPa, the sc-C_{96} is energetically more stable than C_{96} molecule, and the energy barrier from C_{96} molecules to sc-C_{96} is very small (0.023 eV/atom). Hence, the transformation from C_{96} molecules to sc-C_{96} may occur easily under 1 GPa conditions. The detailed atomic process of the transition from C_{96} molecules to sc-C_{96} under 1 GPa is given in Supplemental Fig. S2.

4. Conclusion

In summary, a new 3D carbon allotrope with octahedral symmetry (sc-C_{96}) has been predicted by the first-principles calculations. This new form carbon is energetically metastable and dynamically stable. The electronic structures show that sc-C_{96} is semimetallic and exhibits band crossings phenomena around the Fermi level. The band crossings in sc-C_{96} lead to node-lines Fermi surface in 3D momentum space, which protected by the time reversal and spatial inversion symmetry. In addition, it is found that the SOC strength of sc-C_{96} is small, so sc-C_{96} can be regarded as a new 3D topological nodal line semimetal. Meanwhile, a possible synthetic pathway has been suggested, which indicates that sc-C_{96} may be easily synthesized by polymerizing C_{96} fullerene molecules under low pressure conditions. Once obtained, the fascinating sc-C_{96} would have a wide range of applications in future electronics materials as we expect it can be synthesized by experimentalists.

Acknowledgments

This work was supported by the National Natural Science Foundation of China (Grant No.'s 51121061, 51131002, 51372215), the Key Basic Research Program of Hebei Province of China (Grant No. 12965135D) and the Natural Science Foundation for Distinguished Young Scholars of Hebei Province of China (Grant No. E2013203265). R. M. acknowledges the support from the NSERC and CRC programs, Canada. The authors also would like to thank the staff of the Center for Computational Materials Science, Institute for Materials Research, Tohoku University for computer support. Y. K. is thankful to the Russian Megagrant Project No. 14.B25.31.0030.

Appendix A. Supplementary data

Supplementary data related to this article can be found at http://dx.doi.org/10.1016/j.carbon.2015.11.039.

References

[1] G. Xu, H. Weng, Z. Wang, X. Dai, Z. Fang, Chern semimetal and the quantized anomalous Hall effect in HgCr2Se4, Phys. Rev. Lett. 107 (18) (2011) 186806.
[2] Z. Wang, Y. Sun, X.-Q. Chen, C. Franchini, G. Xu, H. Weng, et al., Dirac semimetal and topological phase transitions in A 3 Bi (A= Na, K, Rb), Phys. Rev. B 85 (19) (2012) 195320.
[3] Z. Wang, H. Weng, Q. Wu, X. Dai, Z. Fang, Three-dimensional Dirac semimetal and quantum transport in Cd 3 As 2, Phys. Rev. B 88 (12) (2013) 125427.
[4] Z. Liu, B. Zhou, Y. Zhang, Z.J. Wang, H. Weng, D. Prabhakaran, S.-K. Mo, Z. Shen, Z. Fang, et al., Discovery of a three-dimensional topological Dirac semimetal, Na3Bi, Science 343 (6173) (2014) 864–867.
[5] Z.K. Liu, J. Jiang, B. Zhou, Z.J. Wang, Y. Zhang, H.M. Weng, et al., A stable three-dimensional topological Dirac semimetal Cd3As2, Nat. Mater. 13 (7) (2014) 677–681.
[6] H. Weng, Y. Liang, Q. Xu, Y. Rui, Z. Fang, X. Dai, et al., Topological Node-line Semimetal in Three Dimensional Graphene Networks, arXiv preprint arXiv: 14112175, 2014.
[7] R. Yu, H. Weng, Z. Fang, X. Dai, X. Hu, Topological Node-line Semimetal and Dirac Semimetal State in Antiperovskite Cu3PdN, arXiv preprint arXiv:

150404577, 2015.
[8] Y. Kim, B.J. Wieder, C. Kane, M. Rappe, Dirac Line Nodes in Inversion Symmetric Crystals, arXiv preprint arXiv:150403807, 2015.
[9] X. Wan, A.M. Turner, A. Vishwanath, S.Y. Savrasov, Topological semimetal and Fermi-arc surface states in the electronic structure of pyrochlore iridates, Phys. Rev. B 83 (20) (2011) 205101.
[10] W. Zdanowicz, L. Zdanowicz, Semiconducting compounds of the AII BV group, Annu. Rev. Mater. Sci. 5 (1) (1975) 301–328.
[11] C.-X. Liu, H. Zhang, B. Yan, X.-L. Qi, T. Frauenheim, X. Dai, et al., Oscillatory crossover from two-dimensional to three-dimensional topological insulators, Phys. Rev. B 81 (4) (2010) 041307.
[12] A.C. Neto, F. Guinea, N. Peres, K.S. Novoselov, A.K. Geim, The electronic properties of graphene, Rev. Mod. Phys. 81 (1) (2009) 109.
[13] A.A. Balandin, S. Ghosh, W. Bao, I. Calizo, D. Teweldebrhan, F. Miao, et al., Superior thermal conductivity of single-layer graphene, Nano Lett. 8 (3) (2008) 902–907.
[14] C. Lee, X. Wei, J.W. Kysar, J. Hone, Measurement of the elastic properties and intrinsic strength of monolayer graphene, Science 321 (5887) (2008) 385–388.
[15] A.K. Geim, Graphene: status and prospects, Science 324 (5934) (2009) 1530–1534.
[16] S. Zhang, Q. Wang, X. Chen, P. Jena, Stable three-dimensional metallic carbon with interlocking hexagons, Proc. Natl. Acad. Sci. 110 (47) (2013) 18809–18813.
[17] S. Zhang, J. Zhou, Q. Wang, X. Chen, Y. Kawazoe, P. Jena, Penta-graphene: A new carbon allotrope, Proc. Natl. Acad. Sci. 112 (8) (2015) 2372–2377.
[18] M. Tagami, Y. Liang, H. Naito, Y. Kawazoe, M. Kotani, Negatively curved cubic carbon crystals with octahedral symmetry, Carbon 76 (2014) 266–274.
[19] L. Jiang, Z. Fan, Design of advanced porous graphene materials: from graphene nanomesh to 3D architectures, Nanoscale 6 (4) (2014) 1922–1945.
[20] Y. Chen, Y. Xie, S.A. Yang, H. Pan, F. Zhang, M.L. Cohen, et al., Spin-orbit-free Weyl-loop and Weyl-point Semimetals in a Stable Three-dimensional Carbon Allotrope, arXiv preprint arXiv:150502284, 2015.
[21] P. Hohenberg, W. Kohn, Inhomogeneous electron gas, Phys. Rev. 136 (3B) (1964) B864.
[22] W. Kohn, L.J. Sham, Self-consistent equations including exchange and correlation effects, Phys. Rev. 140 (4A) (1965) A1133.
[23] G. Kresse, J. Furthmüller, Efficient iterative schemes for ab initio total-energy calculations using a plane-wave basis set, Phys. Rev. B 54 (16) (1996) 11169.
[24] G. Kresse, D. Joubert, From ultrasoft pseudopotentials to the projector augmented-wave method, Phys. Rev. B 59 (3) (1999) 1758.
[25] P.E. Blöchl, Projector augmented-wave method, Phys. Rev. B 50 (24) (1994) 17953.
[26] J.P. Perdew, A. Zunger, Self-interaction correction to density-functional approximations for many-electron systems, Phys. Rev. B 23 (10) (1981) 5048.
[27] Q. Li, Y. Ma, A.R. Oganov, H. Wang, H. Wang, Y. Xu, et al., Superhard monoclinic polymorph of carbon, Phys. Rev. Lett. 102 (17) (2009) 175506.
[28] A. Togo, F. Oba, I. Tanaka, First-principles calculations of the ferroelastic transition between rutile-type and CaCl2-type SiO2 at high pressures, Phys. Rev. B 78 (13) (2008) 134106.
[29] J.P. Perdew, K. Burke, M. Ernzerhof, Generalized gradient approximation made simple, Phys. Rev. Lett. 77 (18) (1996) 3865.
[30] J. Furthmüller, J. Hafner, G. Kresse, Ab initio calculation of the structural and electronic properties of carbon and boron nitride using ultrasoft pseudopotentials, Phys. Rev. B 50 (21) (1994) 15606.
[31] F. Occelli, P. Loubeyre, R. LeToullec, Properties of diamond under hydrostatic pressures up to 140 GPa, Nat. Mater. 2 (3) (2003) 151–154.
[32] F.D. Murnaghan, The compressibility of media under extreme pressures, Proc. Natl. Acad. Sci. 30 (9) (1944) 244–247.
[33] N. Mounet, N. Marzari, First-principles determination of the structural, vibrational and thermodynamic properties of diamond, graphite, and derivatives, Phys. Rev. B 71 (20) (2005) 205214.
[34] Y. Liu, G. Wang, Q. Huang, L. Guo, X. Chen, Structural and electronic properties of T graphene: a two-dimensional carbon allotrope with tetrarings, Phys. Rev. Lett. 108 (22) (2012) 225505.
[35] J. Hass, W. De Heer, E. Conrad, The growth and morphology of epitaxial multilayer graphene, J. Phys. Condens. Matter 20 (32) (2008) 323202.
[36] M.G. Moreno-Armenta, W.L. Pérez, N. Takeuchi, First-principles calculations of the structural and electronic properties of Cu 3 MN compounds with M= Ni, Cu, Zn, Pd, Ag, and Cd, Solid State Sci. 9 (2) (2007) 166–172.